

10

Energy Harvesting

The sensing and design principles we considered so far can have another and crucial application, which is the harvesting of energy from the environment to power the sensors themselves. You may recall that in Chapter 1 I defined sensors as devices that transform one form of energy to another (often to electrical energy). You can see that I have already acknowledged that the environment in which sensors are deployed produces energy that can be used to operate sensors by charging their batteries or energy storage devices. Some environments, such as the human body, produce heat and movement. Researchers have identified several mechanisms by which electrical energy can be harvested from a human body including: use of glucose oxidation, electric potentials of the inner ear, mechanical movements of limbs, and natural vibrations of internal organs (Mitcheson et al. 2008; Ramadass and Chandrakasan 2010; Saha et al. 2008; Vullers et al. 2009). Bridges and water produce continuous ambient movement (vibration) (Beeby et al. 2006, 2007; Stephen 2006); other environments such as open fields, give the opportunity to use solar and wind energy (Kansal et al. 2007; Raghunathan et al. 2005; Sudevalayam and Kulkarni 2011; Taneja et al. 2008). Thermocouples can be used to generate energy from heat (Tan and Panda 2011), piezoelectric devices can be used to generate energy from vibration (Erturk and Inman 2011; Khaligh et al. 2010; Sirohi and Mahadik 2011; Stanton et al. 2010), inductive motors can be used in conjunction with mechanical ambient vibrations to generate energy from the environment, and photovoltaic cells (PN-junction crystalline silicon solar cells) can be used to generate energy from light or solar radiation (López-Lapeña et al. 2010; Qiu et al. 2011, Tan and Panda 2011). Energy can even plausibly be harvested from ambient radio-frequency (RF) radiation (or noise) (Nishimoto et al. 2010; Shi et al. 2011), although this is a very optimistic scenario, as the amount of energy that can be generated from RF sources is extremely small.

10.1 Factors Affecting the Choice of an Energy Source

Whereas the principles of energy harvesting are straightforward, the selection of the appropriate source, nevertheless, should take several factors into account. These preconditions, or the factors affecting the choice of the appropriate energy source, are the following:

- the lifetime of the sensor deployment
- the amount of energy the sensor consumes as a load

- the amount, the predictability, and controllability of the energy that can be harvested
- the capacity and quality of the energy storage device.
- the complexity of the regulation circuit interfacing the energy harvesting, the energy storage, and the sensing systems.

We shall discuss these factors in the following subsections.

10.1.1 Sensing Lifetime

Energy harvesting requires harvesting and regulation components. It also requires harvesting time. Whether or not the effort of designing and deploying energy-harvesting components is worthwhile depends, first and foremost, on how long the components will be used for. The longer the lifetime, the more worthwhile is the cost. Other factors, such as the weight of the harvesting system, should also be taken into account when lifetime is considered. For example, the heat dissipation produced by a harvesting system during excessive charging can cause irritation to a human body and its long-term impact can be detrimental. Likewise, the movement of objects can be constrained when they are loaded with additional components. Therefore, both aspects of deployment lifetime should be taken into account when designing and deploying energy-harvesting systems.

10.1.2 Sensor Load

The sensing system may consist of many components, including sensor(s), conditioning circuits, analogue-to-digital-converter(s), a processor (microcontroller), and, perhaps, a wireless transceiver. The overall power consumption of the sensing system is the sum total of the power consumed by each component. In most practical cases, as the measurand, for which the sensing system is deployed, changes slowly over time, the sensing system can operate in active and inactive states to save energy. The duty cycle of the sensing system can be tuned in accordance with the average amount of power that can be harvested from the environment. Consider, for example, that the average power that can be steadily delivered by the combined effort of the harvesting and storage systems is p_{avg} watts at v_{dd} volts. Hence, the average current that should be drawn by the sensing system should be:

$$i_{\text{avg}} = \frac{p_{\text{avg}}}{v_{\text{dd}}} \quad (10.1)$$

The duty cycle of the sensing system (the alternation between active and inactive states) is defined as:

$$D = \frac{\tau_a}{\tau_a + \tau_{\text{in}}} \quad (10.2)$$

Then, the average power consumption of the sensing system can be expressed as:

$$p_{\text{avg}} = p_a \tau_a + p_{\text{in}} \tau_{\text{in}} \propto i_a \tau_a + i_{\text{in}} \tau_{\text{in}} \quad (10.3)$$

where i_a and i_{in} are the currents drawn by the sensing system when active and inactive, respectively. Assuming v_{dd} remains constant when the current drawn by the sensing system varies, we have,

$$i_{\text{avg}} = i_a \tau_a + i_{\text{in}} \tau_{\text{in}} \quad (10.4)$$

The duration of the active time τ_a can be expressed as a fraction of the duration of the inactive time,

$$\tau_a = \alpha \tau_{in}, \alpha \ll 1 \quad (10.5)$$

Setting the idle time to unity, we have,

$$i_{avg} = \alpha i_{in} + i_a \quad (10.6)$$

α can be fixed according to the application context for which the sensor and the energy harvesting system are deployed:

$$\alpha = \frac{i_{avg} - i_a}{i_a} \quad (10.7)$$

Finally, the duty cycle can be expressed in terms of the average current that should be drawn from the energy-harvesting system:

$$D = \frac{\alpha \tau_{in}}{\alpha \tau_{in} + \tau_{in}} = \frac{\alpha}{\alpha + 1} = \frac{i_{avg} - i_a}{i_{avg} - i_a + i_a} \quad (10.8)$$

10.1.3 Energy Source

There are several vital aspects of the energy source that should be taken into account to decide which source to tap and which harvesting component to design.

The first is the expected amount of energy that can be harvested in a unit time (this refers to the amount of charge that can be accumulated in a unit time at a given voltage) and the rate of fluctuation of the available energy. The latter not only affects the amount of charge that can be collected but also:

- the rate at which the energy storage or the battery should be charged
- the complexity of the regulation component that controls and regulates the charge storage process, which in turn affects the design cost of the energy-harvesting system.

The second aspect is the predictability and controllability of the energy source. Controllability refers to the ability to control both the amount and the timing of energy generation, and predictability refers to the ability to foresee the fluctuation in the amount of energy that can be harvested. Almost all ambient sources (solar, wind, thermal, vibration, and so on) are uncontrollable by nature, but for some specific settings, they can be predictable. Some ambient sources (for example, heat or vibration from a human body) can be considered so deterministic that we can take them for controllable sources. Controllability and predictability intimately influence the choice of the energy-storage system as well as the complexity of the regulation system.

The third aspect is the efficiency with which the energy of the source can be converted to useful energy (electrical energy). A significant amount of energy is lost during conversion: at the interface between the source and the sensing element (the converting element), between the sensing element and the regulator, and in the storage system itself. Table 10.1 provides a compact summary of some of the available energy sources, the sensing elements they use to convert one form of energy to electrical energy, the conversion efficiency, and the obtainable energy.

Table 10.1 A summary of energy harvesting sources, mechanisms, and efficiency

Source	Sensing	Conversion efficiency	Obtainable power
Solar	Photovoltaic cells	16 – 17%	12 mW/cm ²
Ambient indoor light	Photovoltaic cells	16 – 17%	100 mW/cm ²
Thermoelectric	Thermocouple	≤ 1% for $\Delta T < 40^\circ\text{C}$	60 $\mu\text{W}/\text{cm}^2$ at $\Delta T = 5^\circ\text{C}$
Ambient air flow	MEMS turbine	—	1 mW/cm ² at 30 l/min
Wind	Anemometer	59% (theoretical limit)	up to 1200 mW/day
Footfalls	Piezoelectric	7.5%	5 W
Finger motion	Piezoelectric	11%	2.1 mW
Exhalation	Breath mask	40%	0.4 W
Breathing	Ratchet-flywheel	50%	0.42 W
Blood pressure	Microgenerator	40%	0.37 W

A portion of the data is gathered from Paradiso and Starner (2005) and Kansal et al. (2007).

10.1.4 Storage

The storage system in the design and application of an energy-harvesting system plays a vital role. There are two essential aspects that necessitate energy storage. First of all, the amount of energy that can be harvested from the environment fluctuates considerably, and therefore cannot be directly fed to the load (the sensing system). Secondly, there is a discrepancy between the supply of and demand for energy in the sensing system: at times, the load may not consume all the energy a source can provide and at other times the source may not provide the amount of energy the load demands. To deal with these two concerns, the viable solution is to accumulate and store energy, whenever it is available, for later use.

There are various options from which a suitable storage system can be chosen (Winter and Brodd 2004). Broadly speaking, these options can be classified into two groups: special-purpose capacitors (supercapacitors) and rechargeable batteries. Special-purpose capacitors are double-layer electrolytic capacitors that employ a highly porous, ultralight dielectric material having a large surface area (a carbon aerogel) to store charges (Conway 2013, Pandolfo and Hollenkamp 2006, Zhu et al. 2011). These capacitors have much faster charging and discharging rates, much higher power densities, and are more environmental-friendly than their chemical counterparts. However, their energy densities and capacities are significantly smaller. Rechargeable batteries, on the other hand, have relatively high energy density, high capacity, and charge-discharge cycles typically of the order of 200–2000 cycles. But they are more expensive and adverse to the environment. The difference between power and energy densities should be clear. Energy is the capacity to do work. Power is the rate at which energy is consumed or stored. Power can be better understood as the amount of charge that can be accumulated or drawn per unit time. Figure 10.1 compares the energy and power density of rechargeable batteries and capacitors.

There is a wide selection of commercially available rechargeable batteries. The selection criteria include mass–energy-density, volume–energy-density, mass, volume, capacity, self-discharge (leakage), and charging method, among others. The density criteria refer to the amount of energy that can be stored in a unit volume or mass.

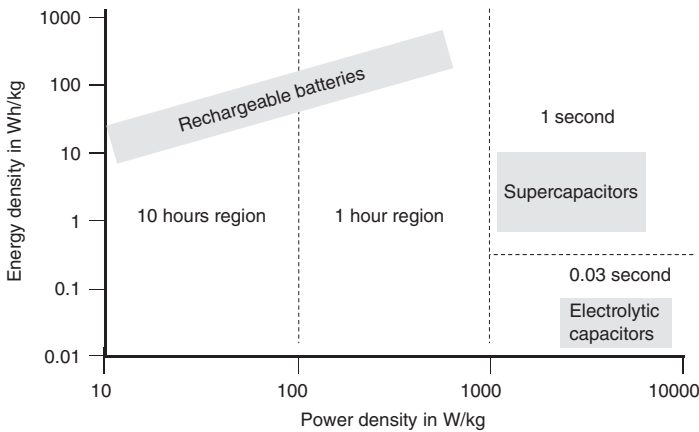


Figure 10.1 A comparison of power and energy densities of rechargeable batteries and capacitors as energy storage systems.

The self-discharging criterion is a measure of the tightness of the storage system to contain the charge it accumulates for a given period of time. Table 10.2 compares the parameters of some commercially available storage systems.

10.1.5 Regulation

The regulator of an energy-harvesting system controls the speed at which the energy storage is charged. It is responsible for protecting the storage system from damage, by controlling the amount of charge with which the storage system is supplied. If desired, a regulator detects when the storage system is fully charged and isolates the storage system from the source to prevent further charging. The complexity of the regulator (and, therefore, its cost) mainly depends on the type of the storage or battery and the charging rate.

The rate at which an energy storage system can be charged is broadly categorised as fast and slow (trickle). The duration of fast charging is typically less than two hours, whereas the duration of slow charging can be indefinite (in other words, the charging current can be applied to the storage indefinitely without damaging it). The maximum amount of slow charging depends on both the chemistry and construction of the internal elements (electrodes and electrolytes). One of the merits of slow charging is that it does not require an extra circuit to detect the completion of charging, because the charging rate is such that the input energy can always be balanced by the output energy supplied to the load. In other words, regulators of trickle charging are relatively cheap. However, care must be taken to ensure that the input and output energies are balanced, otherwise the load (the sensing system) can overload and damage the storage or the regulator if it draws excessive energy.

The amount of current that can be discharged is often expressed as a C-rate, which is a measure of the rate at which a storage system can be discharged (the amount of current that can be drawn from it) relative to its maximum capacity, which is expressed in terms of milliampere hours. A 1C rate corresponds to the discharge of the entire current the storage system can supply in 1 h. For a storage system that has a capacity of 100 mA h, 1C

Table 10.2 A summary of the essential parameters by which commercially available storage systems can be evaluated

Type	Lead acid	NiCd	NiMH	Li-ion	Li-polymer	Supercap
Manufacturer	Panasonic	Sanyo	Energizer	Ultralife	Ultralife	Maxwell
Model number	LC-R061R3P	KR-1100AAU	NH15-2500	UBP053048	UBC433475	BACP0350
Nominal voltage (V)	6.0	1.2	1.2	3.7	3.7	2.5
Energy (Wh)	7.8	1.32	3.0	2.8	3.4	0.0304
Capacity (mAh)	1300	1100	2500	740	930	350 (F)
Mass energy density (Wh/kg)	26	42	100	165	156	5.06
Volume energy density (Wh/L)	67	102	282	389	296	5.73
Mass (g)	300	24	30	17	22	60
Volume (cm ³)	116.4	8.1	8.3	9.3	12.8	53.0
Self-discharge (in % per month)	3–20	10	30	< 10	< 10	5.9 (per day)
Charge-discharge efficiency (%)	70–92	70–90	66	99.9	99.8	97–98
Memory effect	no	yes	no	no	no	no
Charging method	trickle	trickle/pulse	trickle/pulse	pulse ^{a)}	pulse	trickle

a) Pulse charging is a mechanism by which a series of voltage or current pulses is supplied to a storage system. The rise time, width, frequency, and amplitude of the pulses can be controlled to make pulse charging suitable for a variety of size, voltage, capacity, and chemistry. The table is adapted from Taneja et al. (2008).

equates to the discharge of 100 mA in 1 h. A 2C rate of this storage system corresponds to 200 mA h (and, therefore, that the charge will be exhausted in 30 min), and a C/2 rate corresponds to 50 mA h (and, therefore, the charge will be exhausted in 2 h). Most Ni-Cd batteries tolerate sustained charging at a C/10 rate (110 mA h) with no additional protection circuit. In contrast, the slow charging rate for Ni-MH cells is between C/40 (62.5 mA h) and C/10 (250 mA h).

Fast charging has a significantly shorter charge duration, but requires protection circuitry. Moreover, its safety is temperature dependent, with the safest charging temperature for most commercially available batteries often lying between 10 and 40°C and 25°C considered optimal. Without protection circuitry, an excessively charged storage system can internally produce gas, which leads to the recombination of ions, reducing the efficiency of the storage system. The gas in turn builds up pressure within the storage system. Most storage systems are equipped with a venting mechanism that automatically opens to release gas. The opening of the internal vent, however, reduces the lifetime of the battery cell. The type of gas that can be released is chemistry dependent. In Ni-Cd cells, for example, it is oxygen, which is harmless, but for Ni-MH it is hydrogen, which is explosive.

Fast charging may also result in a rapid build up of pressure within a cold storage system. Interestingly, the charging reaction of different storage systems can be different.

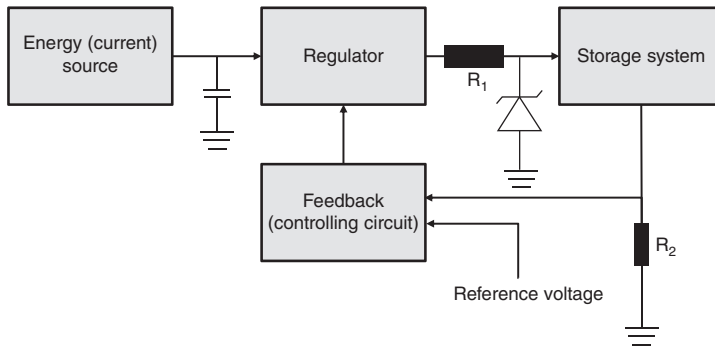


Figure 10.2 A feedback regulator charges an energy storage with a constant current. The feedback system establishes a voltage drop at one of its terminals by tapping a portion of the current entering into the storage system and comparing the voltage drop with a reference voltage to detect overcharging.

For instance, in Ni-Cd cells, the charging reaction is endothermic, which means that charging makes the battery cell colder. In Ni-MH cells, however, the charging reaction is exothermic, which means it increases the temperature of the battery cell. Consequently, Ni-Cd cells tolerate higher rate charging than Ni-MH. Another factor that affects fast charging is the internal resistance of the storage system, because the internal dissipation of power in the form of heat is a function of the internal resistance: $P = I^2R$.

Figure 10.2 shows the basic components of a fast-charging regulator. The main purpose of the regulator is ensuring the constant flow of current into the energy storage. The capacitor between the energy source and the regulator prevents a sudden change of voltage at the source whereas the Zener diode (which is reverse biased) between the regulator and the storage system keeps the charging voltage at a fixed level. When the charging current exceeds its specified limit, a reverse-biased current begins to flow through the Zener diode, thereby reducing the voltage across the storage system. A portion of the current entering into the storage system is tapped to create a voltage drop across one of the terminals of the feedback system (R_2), which is then compared with a reference voltage. If the voltage drop exceeds the reference voltage, the feedback system generates an output voltage to turn off the regulator.

The protection circuit in Figure 10.2 does not take the temperature of the storage system into account. The temperature of the storage system can be a direct indication of the extent to which the storage system is charged. Figure 10.3 displays the temperature-vs-voltage curve for two technologies (Ni-Cd and Ni-MH). As can be seen, the temperature of the two battery technologies steadily increases as the charging nears completion, although obviously the two technologies have different temperature footprints (Ni-Cd does not show any appreciable temperature increment until the battery is fully charged – recall that the internal charge reaction in Ni-Cd is endothermic – whilst a steady increase can be observed from the outset for the Ni-MH). Common to both technologies, however, is a rise in temperature by approximately 10°C as the battery cells are fully charged.

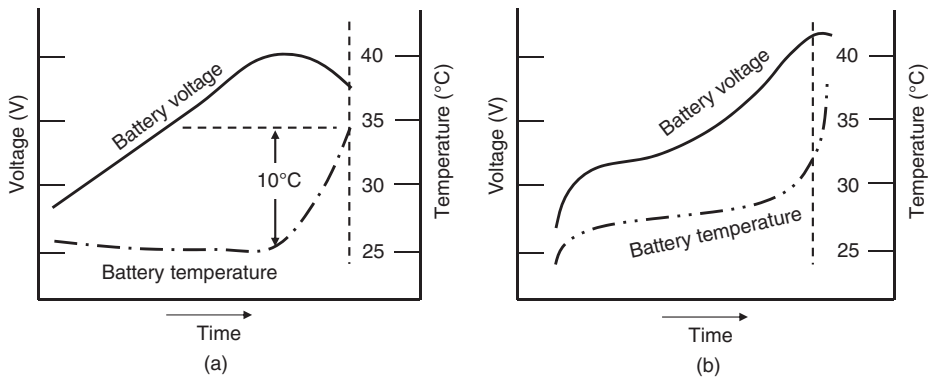


Figure 10.3 Voltage-versus-temperature curves for two different battery cells: (a) Ni-Cd; (b) Ni-MH. The curves were drawn on the basis of measurements taken at a 1C charging rate at 25 °C. As can be seen, the temperature of the batteries significantly rises when the batteries are nearly fully charged. Courtesy of Chester Simpson, National Semiconductor.

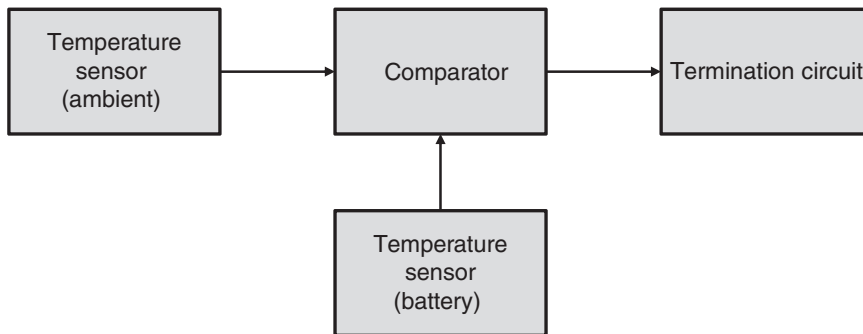


Figure 10.4 ΔT detector for a fast-charging regulator. The temperature of the battery is compared with the ambient temperature to extract the change in temperature due to charging. Often a timer is used in conjunction with the ΔT detector to make sure that the termination signal is generated after the rapid rise in temperature is detected.

Figure 10.4 shows the schematic diagram of a temperature-sensitive end-of-charge detector. Two temperature sensors are used: one to sense the ambient temperature surrounding the storage system as a reference, and the other to directly sense the temperature of the storage system. When the comparator senses a difference of $\Delta T = 10^\circ\text{C}$, it generates a termination signal that turns off the regulator. The temperature sensors output a voltage that is proportional to the rise in temperature. For example, the Texas Instruments LM35 temperature sensor generates $10\text{ mV }^\circ\text{C}^{-1}$. Consequently, a voltage of 100 mV should correspond to $\Delta T = 10^\circ\text{C}$.

Example 10.1 One of the tasks of a voltage regulator is to supply the load with the appropriate DC voltage. Suppose the voltage that can be supplied by the storage system is 3.7 V but the voltage the sensing system requires is 2.3 V. Propose a voltage regulator that converts the 3.7 V supply voltage to 2.3 V load voltage.

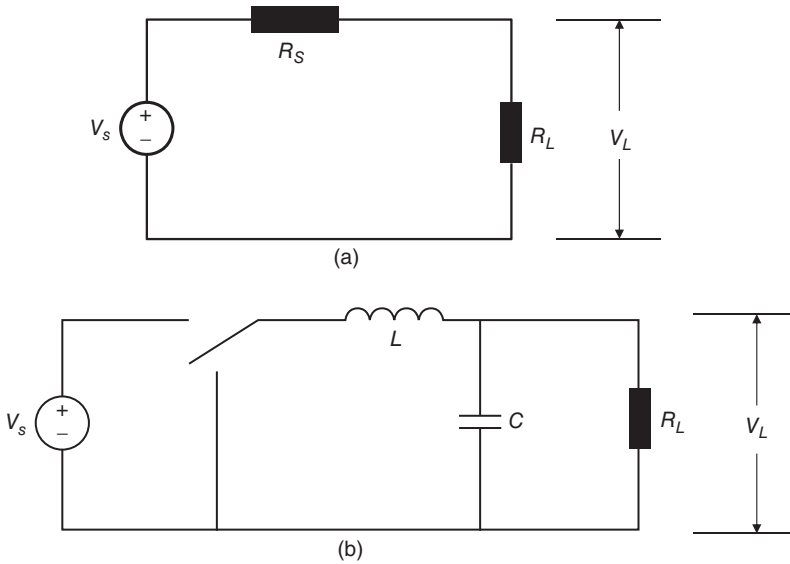


Figure 10.5 A DC-DC converter: (a) a simple but lossy resistive DC-DC converter; (b) a buck converter consisting of a switching device and a low-pass filter. The low-pass filter suppresses the AC component from reaching the load whereas the switching device fixes the duty cycle of the source voltage.

Obviously, what we need is a DC-DC converter. The simplest DC-DC converter would be a single-stage voltage divider circuit, as shown in Figure 10.5a, for

$$V_L = \frac{R_L}{R_L + R_S} V_s \quad (10.9)$$

Since the load resistance is known, it is possible to adjust the source resistance such that the desired voltage can be obtained. However, when a load current flows through the source resistance, there will be a power loss the magnitude of which equals: $P_S = I^2 R_S$. This is rather a waste. The more efficient DC-DC converter is the one shown in Figure 10.5b, which is called a buck converter. Ideally it should be lossless because the capacitor and the inductor are energy-storage components, but they have internal resistance as a result of which there is a small amount of power dissipation in the form of heat. Moreover, because they are imperfect energy storage, they leak, which is why we should expect some inefficiency when we employ voltage regulators. First we shall analyse the circuit logically in order to understand how it works, and then we shall derive the mathematical equations to establish a relationship between the source and load voltages.

The switching component acts as a single-pole, double-throw switch. When the switch is “on” (when it is connected to the source), a DC current flows through the load. Because the inductor acts as a short circuit to DC, ideally there is no voltage drop across the inductor. Likewise, since the capacitor acts like an open circuit for DC, there will be no current branching off into the capacitor, as a result of which all the current generated in the circuit passes through the load, which is what we want. When, however, the switch is “off”, the source is decoupled from the load and, as a result, there will be no current flowing into the load coming from the source. However, since the capacitor has been

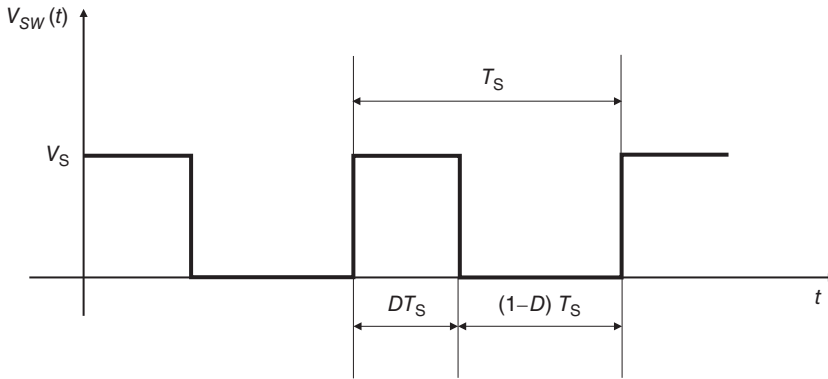


Figure 10.6 The duty cycle of a DC-DC converter.

charging in the previous cycle, now it will discharge through the load and it acts as a current source. Subsequently, the average voltage, consisting of the voltage due to the source from the previous cycle and the voltage due to the discharging capacitor in the present cycle, should provide the desired load voltage.

Suppose we periodically switch “on” and “off” the switch. Furthermore, suppose the duration of the switch in the “on” state is DT_s and in the “off” state is $(1 - D)T_s$ where T_s is the switching period and $\{D : 0 < D < 1\}$ is defined as the duty cycle of the regulator, as can be seen in Figure 10.6. Thus the switching frequency of the DC-DC converter is:

$$f_s = \frac{1}{T_s} \quad (10.10)$$

One of the consequences of the periodic switching is that the voltage across the switch, $V_{SW}(t)$ contains high-frequency components. However, if we choose the cut-off frequency (f_c) of the low-pass filter carefully (by making it significantly smaller than the switching frequency), then it is possible to suppress the high-frequency components:

$$f_c = \frac{1}{\sqrt{LC}} \ll f_s \quad (10.11)$$

The DC component of V_{SW} can be determined by using the inverse Fourier transform:

$$V_{SW}(t) = \frac{1}{T_s} \int_0^{T_s} V_{SW}(j\omega) e^{j\omega t} dt \quad (10.12)$$

Since we are interested in the DC voltage ($\omega = 0$), we can reduce the above expression as follows:

$$V_{SW} = \frac{1}{T_s} \int_0^{DT_s} V_S dt = DV_S \quad (10.13)$$

For our case, $V_{SW} = 2.3$ V and $V_S = 3.7$ V. Hence,

$$D = \frac{2.3}{3.7} \approx 0.62$$

10.2 Architecture

So far, we have seen how different factors can affect the design of an energy-harvesting system. The architecture of this system, both the choice of building blocks and how the building blocks should be interconnected, is likewise influenced by those factors. Conceptually speaking, however, it is possible to identify the most significant components and to determine the input-output relationships between these components, as shown in Figure 10.7. Since we are interested in supplying energy to a sensing system, there are understandably two types of measurand: the first is the main physical process or object for which the sensing system is designed whilst the second is our energy source. The two may or may not be similar. Even when they are similar, the sensing techniques we employ are essentially different, as the outputs of the two systems are different.

The energy sensor (or converter) transforms the physical quantity (radiation, wind, heat, vibration, and so on) to electrical power. The sensor is typically characterised by its conversion efficiency and suitability with respect to the sensing system in terms of its size, weight, and the amount of heat it produces. Since the sensing system is typically small, the energy harvester, when compared to its macro counterparts, is typically small as well, which means the issues we raised and discussed in Chapter 9 as regards miniaturisation concern us here. One of the crucial problems with miniaturised energy harvesting is that the efficiency of the converter decreases as its size decreases.

In general there are two regulators. One of them (the input regulator) conditions the output of the energy converter to meet the operational requirements of both the storage and the sensing systems. For example, the output voltage and current of the converter may not match the input voltage and current requirements of the storage system, in which case the regulator adjusts the output voltage and current to meet the requirement. As we have already seen, the input regulator also manages the charging process of the storage system. Similarly, the output regulator conditions the output of the storage system and the input regulator to meet the operational requirements of the sensing system. The essential difference between the input and the output regulators is that whereas the charging current of the storage system is constant, the operational current of the load varies, depending on its activity level. The activity level, in turn, depends on the complexity of the sensing system. If the sensing system integrates a processor, then, the amount of current it draws from the output regulator significantly varies with the variation of the processor's current state. For example, Table 10.3 displays the nominal

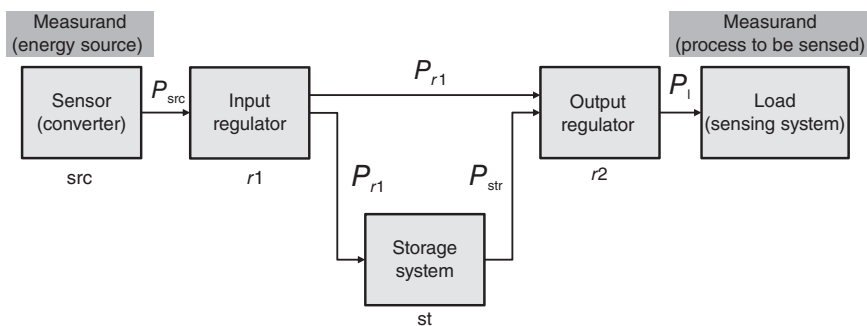


Figure 10.7 The main components constituting the architecture of an energy-harvesting system.

Table 10.3 Nominal current draw of the ATmega128L Microcontroller

Power mode	Current (mA)
Active	8.0
Idle	3.2
ADC noise reduction	1.0
Power-down	0.103
Power-save	0.110
Standby	0.216
Extended standby	0.223

current an ATmega128L microcontroller draws in different power modes (Dargie 2012). Consequently, the output regulator should be able to provide different amounts of current to the sensing system and protect the storage system from overload.

When the available energy source is inadequate to directly supply power to the sensing system (load), the storage system has to charge first. However the energy source may have a surplus of energy available to directly supply the load with power whilst the storage system is charged. In this case, the input regulator should meet the demands of the storage system as well as of the output regulator. The overall efficiency of the energy-harvesting system depends on the efficiency of the input and output regulators as well as of the storage system (itself dependent on the self-discharge rate of the storage system). Hence,

$$\eta = \eta_{\text{src}} \times \eta_{\text{r1}} \times \eta_{\text{str}} \times \eta_{\text{r2}} \quad (10.14)$$

Equation (10.14) plays a useful role in the design of an energy-harvesting system because it easily relates the power that is required by the load (P_l) to the power that can be supplied by the source (P_{src}):

$$P_l = \eta \times P_{\text{src}} \quad (10.15)$$

Alternatively,

$$P_{\text{src}} = \frac{1}{\eta} \times P_l \quad (10.16)$$

Example 10.2 We wish to design a power supply system that harvests energy from blood pressure and uses 300 mg of lithium polymer as its storage system. Suppose the storage system has a self-discharge rate of 2 %, both the output and the input regulators have 50 % efficiency, and the sensing system requires 20 mW of power, how much power should the energy source deliver?

According to Table 10.2, up to 0.37 W can be harvested from the blood pressure with a conversion efficiency of 40 %. Hence we have:

$$\eta_{\text{src}} = 0.4$$

$$\eta_{\text{r1}} = 0.5$$

$$\eta_{st} = 0.98$$

$$\eta_{r2} = 0.5$$

And,

$$\eta = 0.4 \times 0.5 \times 0.98 \times 0.5 = 0.098$$

Therefore, the amount of power the energy source should deliver is:

$$P_{src} = \frac{1}{\eta} \times P_l = \frac{1}{0.098} \times 20 \text{ mW} = 204 \text{ mW}$$

If we assume a 10 % error in our modelling, the maximum power consumed by the sensing system would still be 224.4 W, which is below 370 mW, which can be obtained from the energy source.

10.3 Prototypes

At the macro scale, the use of renewable energy is becoming to be a ubiquitous phenomenon around the world. As of July 2015, statistics from the European Wind Energy Association (EWEA) reveal that:

In the first six months of 2015, Europe fully grid connected 584 commercial off-shore wind turbines, with a combined capacity totalling 2342.9 MW. Additionally, 15 commercial wind farms were under construction. Once completed, these wind farms will have a total capacity of over 4268.5 MW.¹

At the macro scale, however, harvesting energy is not as ubiquitous. In this section, we shall consider some representative prototypes.

10.3.1 Microsolar Panel

A simple crystalline PN-junction crystalline silicon is the basis for constructing a solar panel to transform light energy into electrical energy. Silicon is a semiconductor and therefore has four electrons in its outer orbit. Atoms in a silicon crystal form a covalent bond to get eight electrons in their outer orbit, which makes the crystal stable. When considered separately, each silicon atom is electrically neutral, as the number of electrons (which are negatively charged) and protons (which are positively charged) are always equal. So crystalline silicon is also electrically neutral. Incidentally, metals also have equal numbers of electrons and protons, but the electrons in the outer orbits of metals, which are always less than three, are loosely held or attracted by the positive nucleus, as a result of which they can be easily excited out of their orbits.

A non-metal atom, such as phosphorus, which has five electrons in its outer orbit, can be injected into a silicon crystal by a process known as doping. The process does not immediately change the electrical neutrality of the now doped crystalline silicon, as the number of electrons and protons are still equal, but it creates the necessary condition to make it unstable. Similarly, a metal atom, such as boron, with three electrons in its

¹ Source: European Wind Energy Association (2016).

outer shell, can also be injected into the silicon crystal to create the necessary condition for an electrical imbalance. The quantity of dopant (impurities) in the crystalline silicon significantly influences its electrical properties. When the crystal is doped lightly, it is often referred to as extrinsic semiconductor because its semiconductor property dominates; in contrast, when the crystal is highly doped, it behaves more like a conductor rather than a semiconductor and is referred to as a degenerate semiconductor.

Now consider Figure 10.8. Suppose we first have an undoped crystalline silicon as shown in (a). On the left-hand side of part (b), an N-type crystal is doped with atoms which have five outer electrons. Each silicon atom contributes four outer electrons. So in the neighbourhood of the dopant, there are altogether nine outer electrons, eight tightly held by a covalent bond, but one free to move. The more impurities there are, the more free electrons there will be. Similarly, on the right-hand side of part (b), an N-type crystal is doped with atoms having three electrons. Therefore, in the neighbourhood of this atom, there are only seven electrons, with a deficiency of one electron to make that region stable (in a sense, there is a positively charged hole in this region into which a single electron can fall).

When an N-type and a P-type crystal are physically brought together, an interesting phenomenon occurs. The free electrons in the N-type crystal will be accelerated towards

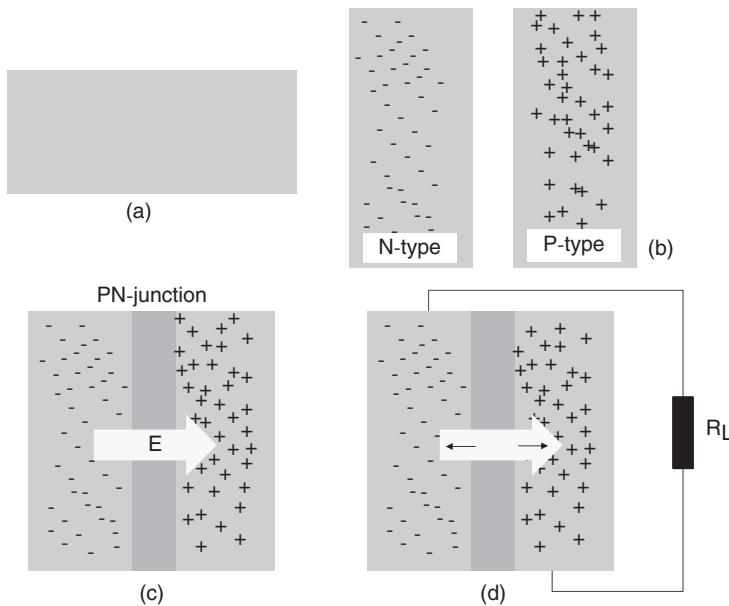


Figure 10.8 The formation of a PN-junction is the basis for the construction of a crystalline silicon solar panel: (a) a pure crystalline silicon in which silicon atoms form covalent bonding to form the crystal; (b) negatively and positively doped crystalline silicon. In both cases, the doped silicon, when separately considered, is electrically neutral, as the number of positively charged and negatively charged particles are equal, effectively cancelling each others' charges; (c) the combination of N- and P-type crystals enables some of the free electrons in the N-type crystal to migrate to the P-type crystal in order to combine with some of the positive charges – this way, the net charge density in the N-type crystal becomes positive and the net charge density in the P-type crystal becomes negative and the charge imbalance creates an electric field; (d) a closed circuit formed by an external load resistance enables the flow of current due to the charge concentration imbalance in the PN-junction solar panel.

the P-type crystal to fill up the deficiency there. In doing so, however, now that they have left their original crystal, there will be an imbalance between the electrons and protons in the N-type crystal (the net charge of the crystal will be positive). Similarly, there will be an imbalance in the P-type crystal with the P-type crystal becoming negative. As can be seen in part (c), the charge imbalance in these regions creates an electric field, the strength of which depends on the rate at which free electrons initially migrate and the concentration of dopant in both regions. The tendency of this field is to oppose the further migration of electrons and holes across the PN-junction.

Meanwhile, what happens when energy of some kind frees some of the electrons in the PN junction? They will be accelerated by the electric field towards the N-type crystal, while the free holes will be accelerated towards the P-type crystal. If the circuit is closed, as shown in Figure 10.8d, then the accelerated electrons will repel some of the free electrons in the N-type crystal whilst their counterparts, the accelerated holes, will repel some of the holes in the P-type crystal. The repelled electrons and holes in their turn repel other electrons and holes, and so the propagation of electrons and holes will continue towards the edges and through the connecting wires, and this way, a flow of electrons (a current) will be created.

A crystalline silicon (c-Si) solar cell is essentially a PN-junction semiconductor that releases electrons when the PN-junction is exposed to radiation. A moderately doped P-type square wafer is used as an absorber material. Its typical dimensions are 10×10 cm and a thickness of approximately $300 \mu\text{m}$. Both sides of the wafer are highly doped: the top N-type and the bottom P-type. The solar panel is organised into cells, modules, and arrays (as shown in Figure 10.9). The power that can be generated by a single cell is essentially small, but by connecting multiple cells in series modules can be formed. These are usually a sealed or encapsulated unit of convenient size. Similarly, when multiple modules are connected, they form arrays. The power generated by solar panels is environmentally friendly, because the panels produce no air, thermal, or water pollution. The only disadvantage of solar panels at present is their high cost and the fact that the production process has a negative environmental impact, primarily from the energy required. A small amount of heavy metals (typically lead and cobalt) are also produced in the purification of crystalline silicon.

Taneja et al. (2008) at UC Berkeley implemented the architecture by employing a micro-solar panel (see Figure 10.7). They began their design by first analysing the power requirement of their sensing system, which consists of sensing, processing, and radio subsystems. The purpose of the sensor node was “to collect widespread, high-frequency, and automated observations of the life cycle of water as it progresses through a forest ecosystem”. The sensor node can be configured to operate with different duty cycles. For their purposes, it was enough to operate the processor with a 0.4% and the radio with a 1.2% duty cycle. The peak active current the node draws when the processor is on and the radio is in receiving mode is 0.53 mA at 3.3 V. The node draws $15 \mu\text{A}$ when sleeping.

Their selection of the input and output regulators as well as the storage system was primarily influenced by cost and the efficiency with which power could be transferred from the solar panel to the storage system. The solar panel matching the size of their sensor node was a 4 V, 100 mA panel from Silicon Solar Inc. This panel delivers a maximum output power of 276 mW h at 3.11 V. The authors argue that experimenting with an input regulator showed that the panel was forced to operate at a point far from its

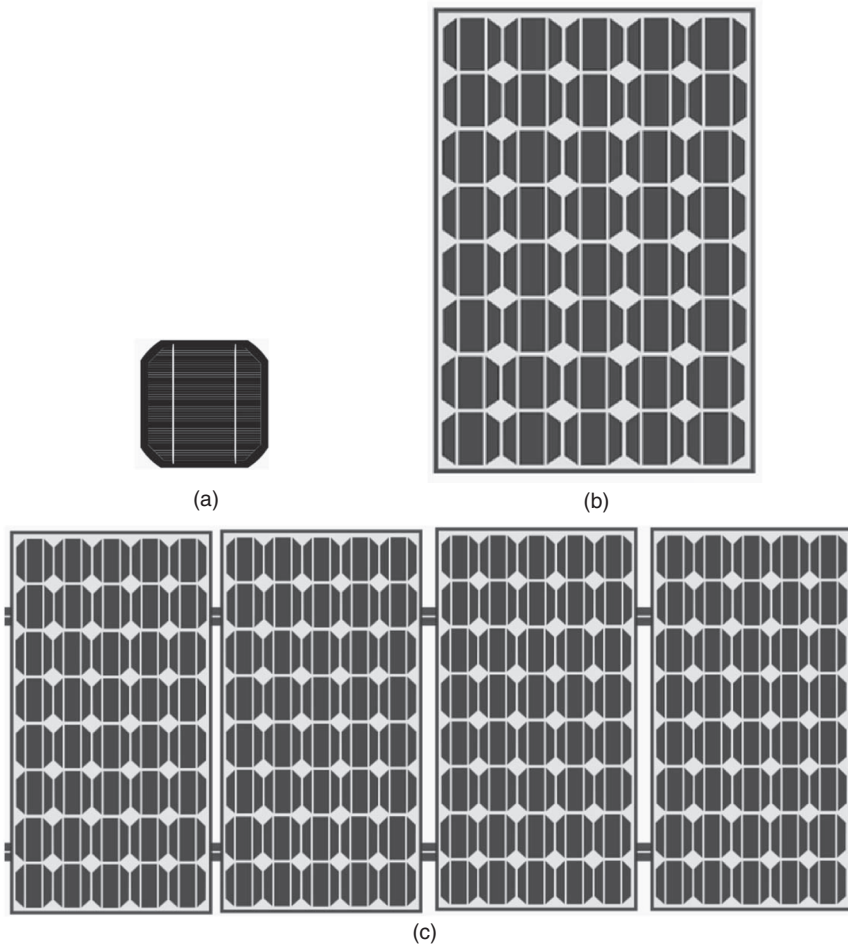


Figure 10.9 The components of a solar (photovoltaic) panel: (a) a single cell; (b) a single module; (c) an array of modules.

maximum power point. Therefore, they decided to directly supply the output of the solar panel to the storage system.

Their choice of storage system took into consideration the simplicity with which it could be integrated into their overall system. For this reason, they decided on Ni-MH cells, with $\eta_{st} = 0.66$. Similarly, in their decision regarding the output regulator, the researchers took into account the operating ranges of the storage system and the sensing system (the load). With two Ni-MH AA batteries, the nominal operating voltage of the storage system should be 2.4 V. However, the operating voltage of the sensing system varied between 2.7 and 3.6 V. Therefore, the output regulator had to be able to boost the voltage of the storage system. The output regulator was set up to provide a stable supply voltage. Finally, the authors chose an LTC1751 regulator which, unfortunately, has an efficiency of only 50% ($\eta_{r2} = 0.5$).

Going backward, with the sensing system having an average daily energy requirement of approximately 45.3 mW h and the output regulator having a 50% efficiency, the

storage system had to deliver 79.2 mW h. Thus the input power to the storage system had to be:

$$P_{src} = \frac{1}{\eta_{str}} \times P_{str} = (1/0.66) \times 79.2 \text{ mW h} = 120 \text{ mW h}$$

According to the researchers, the solar panel generates 139 mW h per day if it receives 30 min sunlight per day. Figure 10.10 shows the prototype they designed and deployed at the Angelo Reserve in Northern California. Altogether, the authors deployed 19 nodes over a 220 m × 260 m area stretching across a deep ravine.

10.3.2 Microgenerator

The principle of an electric generator is straightforward and obeys Faraday's electro-magnetic induction law (more precisely, Maxwell-Faraday's equation). If two magnets are placed near one another, as in Figure 10.11, a magnetic field will be set up between

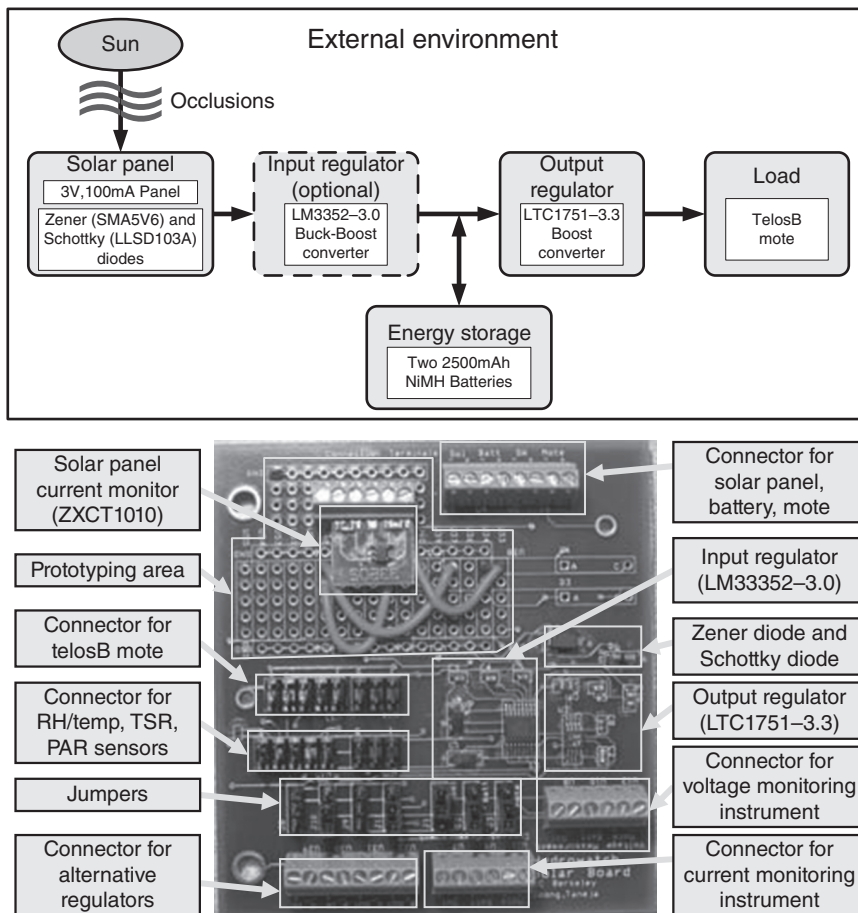


Figure 10.10 A wireless sensor node prototype using a solar panel to harvest energy from sunlight. Courtesy of Taneja et al. (2008) (*Proceedings of the 7th International Conference on Information Processing in Sensor Networks*, IEEE 2008).

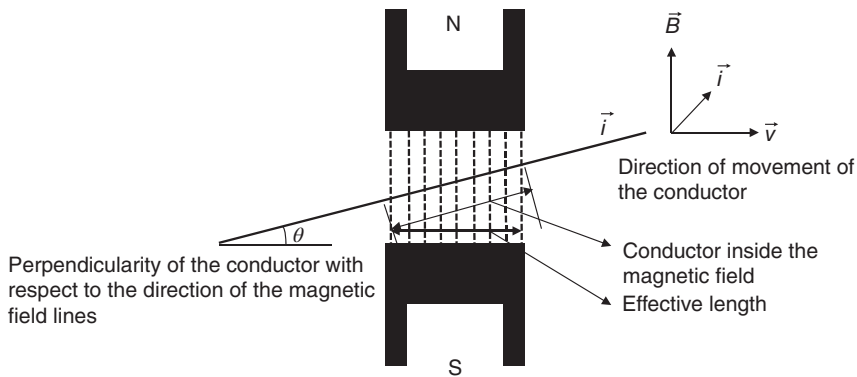


Figure 10.11 The basic principle of an electric generator. A conductor moving inside a magnetic field induces an electric current within itself. The magnitude and direction of the induced current depend on the effective length of the conductor inside the magnetic field, the relative direction of the movement of the conductor with respect to the direction of the field, and the strength of the magnetic field.

them. The magnetic lines of force are always directed from a north pole to a south pole. If a simple conductor of length l moves inside the magnetic field (assuming the conductor makes a complete loop), an electric current will be induced in the conductor and begins to flow. Alternatively, the conductor can be stationary and the two magnets can be moving. In either case, the magnitude of the current depends on the following factors:

- the effective length of the conductor
- the relative position of the conductor with respect to the magnetic field (the component of the conductor which is perpendicular to the magnetic field)
- the speed of the conductor
- the magnetic field strength.

Similarly, the direction of the flow of current depends on the direction of the movement of the conductor with respect to the direction of the magnetic field. In order to produce an appreciable amount of current, the effective length of the conductor must be long. This can be achieved by winding a long wire around a ferromagnetic material. The wristwatch industry has been effectively exploiting this simple principle for more than half a decade. It employs the movement of wrists to move the rotor of the microgenerator to which permanent magnets are attached. The moving magnetic field induces a voltage in the stationary coils of a stator. The AC voltage thus generated is then supplied to an AC-DC converter, which produces a DC current that drives a DC motor.

As can be seen in Figure 10.12a, the ETA Autoquartz watch uses a micromotor and an electronic system to manage the movements of the hour, minute, and second hands. The storage capacitor (accumulator) provides the motor with DC electrical power. It is charged itself by the microgenerator, which produces current as a result of the movement of the wrist. The proof-mass on top of the generator oscillates when the wrist is moved, thereby moving the rotor of the generator. The Seiko system has similar building blocks to generate electrical power using an oscillating proof-mass and to temporarily store the power for regulatory purpose. The proof-mass is conditioned to move in one dimension only (for example, along the x -axis), but the direction of movement along

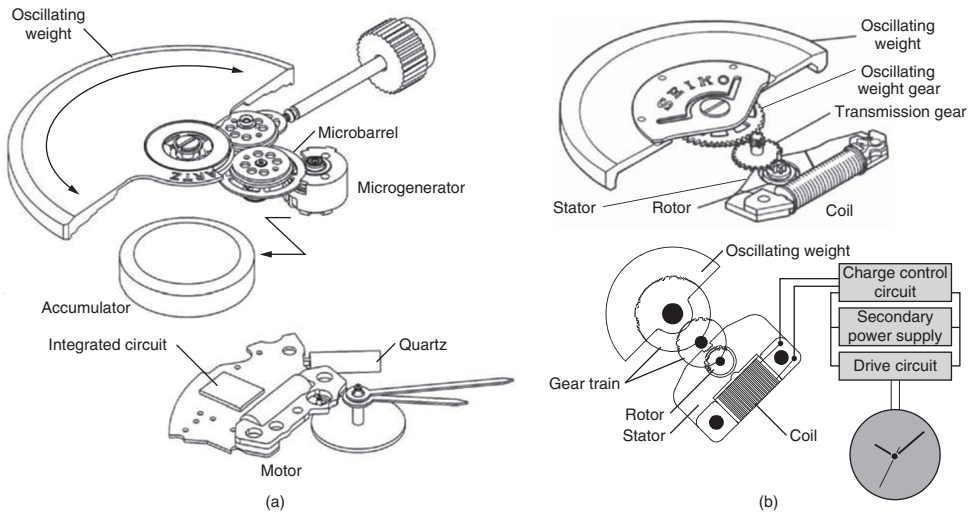


Figure 10.12 Commercially available self-winding mechanisms for micro-generators. (a) Self-winding system for the ETA Autoquartz. The proof-mass winds a spring that pulses the micro-generator at an optimal rate of 15,000 RPM for 50 ms, producing 6 mA at a voltage greater than 16 V. The electric power produced by the microgenerator charges a capacitor, which serves as the energy storage of the Autoquartz. (b) The self-winding mechanism of Seiko's automatic generating system. The mechanism omits the intermediate spring and produces $5 \mu\text{W}$ on average from an ambient movement (when the wristwatch is worn) and 1 mW when the wristwatch is forcibly shaken. Courtesy of Paradiso and Starner (2005), *IEEE Pervasive Computing* 2005.

that axis (left or right) does not matter, because full-wave rectifiers can be used to convert the AC voltage produced as a result of the left-right movement of the proof-mass into a DC voltage.

The sensor and MEMS research community is attempting to take advantage of similar approaches to fabricate microgenerators to supply microelectromechanical sensors with power. Beeby et al. (2007) designed and fabricated a microgenerator with a stationary coil and a moving cantilever, on the top and bottom of which high-density magnets were bonded. The magnets are produced from sintered neodymium iron boron (NdFeB). Cyanoacrylate is used to bond the magnets to the cantilever. Each magnet has dimensions of $1 \times 1 \times 1.5$ mm, the longer dimension (1.5 mm) being normal to the magnetic field. The way the magnets are arranged produces a concentrated flux gradient through the stationary coil as they vibrate. The free end of the cantilever is connected with tungsten wires to provide it with additional mass. The density of the magnet is 7.6 g cm^{-3} . Figure 10.13 shows the dimensions of the cantilever.

The researchers introduced slots and holes into the beam to accommodate the coil and bolt. Moreover, the corners of the beam are shaped so as to reduce the effect of concentrated stress. The cantilever was fabricated from double-polished, single-crystal silicon wafers. The cantilever produced a resonance (vibration) frequency of 50 and 60 Hz when its thickness was $40 \mu\text{m}$. The cantilever beam was fabricated with deep reactive ion etching through the $50 \mu\text{m}$ thickness, and the wafers were resist bonded to a host wafer. The cantilever beam assembly was clamped onto the base using an M1-sized nut and bolt and a square washer, the square washer giving a straight clamped edge

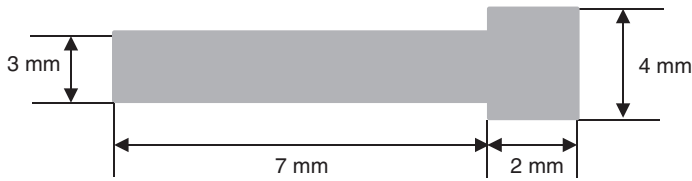


Figure 10.13 The dimensions of the cantilever (the rotor of the microgenerator) to which the high energy density magnets are attached.

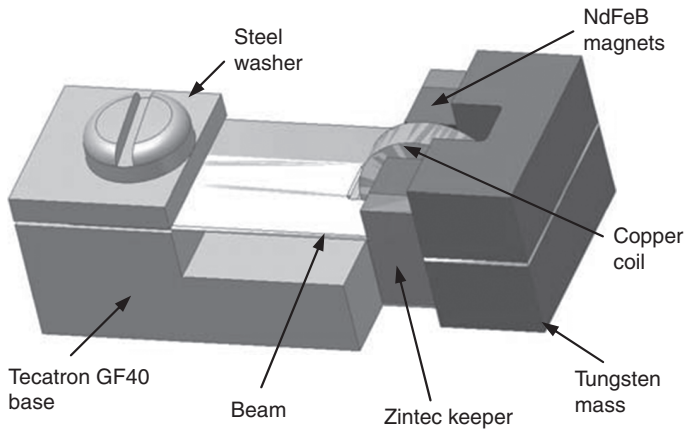


Figure 10.14 The architecture of the cantilever-based microgenerator, which produces an electric power from an ambient vibration. Courtesy of Beeby et al. (2007), *Journal of Micromechanics and Microengineering* (2007).

perpendicular to the beam length. Similarly, the stationary coil was manually bonded to a semi-circular recess machined in the base. It had an outside radius of 1.2 mm, an inside radius of 0.3 mm and a thickness of 0.5 mm. It was wound from 25 μm diameter enamelled copper wire and had 600 turns. Figure 10.14 shows the architecture of the micro-generator.

The researchers report that the micro-generator produced $46 \mu\text{W}$ in a resistive load of $4 \text{ k}\Omega$ when the cantilever received an acceleration of 0.59 m s^{-2} at a resonance frequency of 52 Hz. A voltage of 428 mV (RMS) was obtained from the generator with a 2300-turn coil. The efficiency of the generator was reported to be 30% (that is, 30% of the power supplied from the environment was transformed to useful electrical power in the load).

10.3.3 Piezoelectricity

In piezoelectric energy harvesting, a mechanical vibration can be directly converted to electrical energy, with no need for an intermediate stage. This is because when the atomic structure of piezoelectric materials (such as crystals or certain ceramics) is compressed (strained), an electric charge accumulates in the material producing a potential difference. The amount of energy that can be harvested this way is typically small (in the microwatt range), but it can be sufficient to power MEMS sensors.

Scientists at universities and research centres in the US and China have identified several medical applications for which the energy harvested from piezoelectric materials can be useful. These are heart rate monitors, pacemakers, implantable cardioverter defibrillator (ICD), and neural stimulators (Dagdeviren et al. 2014). The scientists indicate that existing technologies for these devices (bioelectronic devices) require batteries to provide continuous diagnostics and therapy, but the operational lifetime of these batteries is inherently short (a few days for wearable devices and a few years for implants) due to practical constraints. Consequently, surgical procedures are required to replace the batteries of implantable devices, which may expose patients to health risks, heightened morbidity, and even potential mortality; moreover it is needless to state that surgical procedures are costly.

The researchers proposed and developed a piezoelectric harvester to produce energy from the normal rhythms of the heart and the lungs. The structure of the basic element of the harvester consists of a lead zirconate titanate (PZT) ribbon, which is sandwiched between two electrodes, thus forming a capacitor-like structure. The PZT ribbon has a thickness of 500 nm and width and length of 100 μm and 2.02 mm respectively. It is produced by wet chemical etching on a silicon wafer. The top electrode, which has dimensions of 50 μm \times 2 mm, was formed by the deposition of Au/Cr (200 nm/10 nm) with an electron beam evaporator on the surface of a multilayer stack of $\text{Pb}(\text{Zr}_{0.52}\text{Ti}_{0.48})\text{O}_3/\text{Pt}/\text{Ti}/\text{SiO}_2$ (500 nm/300 nm/20 nm/600 nm) on a silicon wafer. The bottom electrode (Pt/Ti) has dimensions of 140 μm \times 2.02 mm and was patterned by wet chemical etching.

A further encapsulation process of the assembly using polyimide (PI), a biocompatible material, isolates the harvester from bodily fluids and tissues and minimises the risks of failure or an immune response. The researchers report that the entire structure is highly flexible, with computed bending stiffnesses (per unit width) of 0.22 N.mm and 0.10 N.mm for regions coincident with and away from the PZT structures, respectively. For a bending radius of 2.5 cm, the researchers reported a maximum strain in the PZT of 0.1 %. Figure 10.15 shows the structure of the piezoelectric harvester, an optical

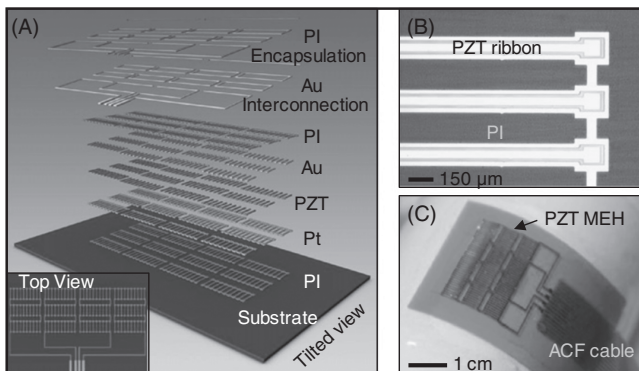


Figure 10.15 A flexible piezoelectric energy harvester: (A) a schematic illustration of the components consisting of the piezoelectric harvester, namely, a piezoelectric ribbon sandwiched between two electrodes and encapsulated within polyimide (PI); (B) an optical microscopic image of PZT ribbons fabricated onto a thin film of PI; (C) image of the entire harvester. MEH, mechanical energy harvester. Courtesy of Dagdeviren et al. (2014), *PNAS* (2014).

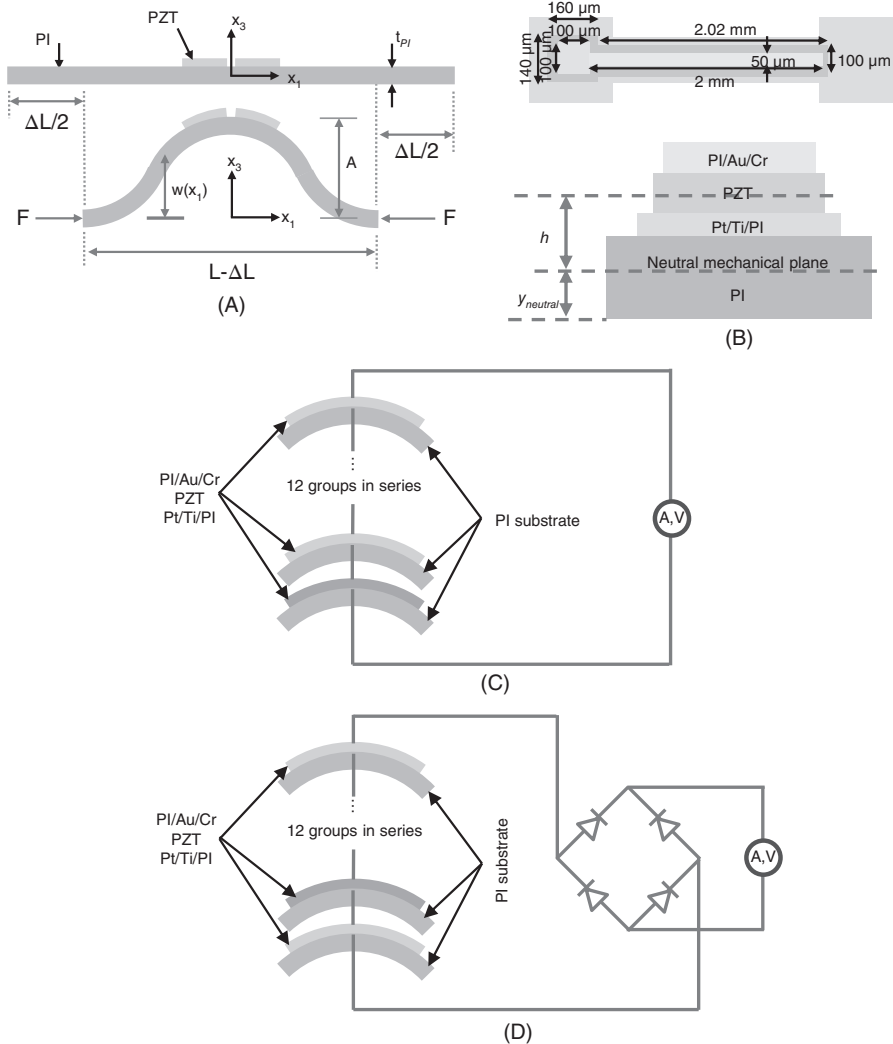


Figure 10.16 Schematic illustrations of the layout of the piezoelectric energy harvester: (A) the theoretical shape for buckling the PZT harvester under compression; (B) a top view of a single PZT ribbon capacitor structure (top), and a cross-section showing the position of the neutral mechanical plane of the device (bottom). A buckled array of PZT ribbon capacitor structures on a PI substrate: (C) without a rectification circuit and (D) with a rectification circuit. Courtesy of Dagdeviren et al. (2014), *PNAS* (2014).

microscope image of the PZT ribbons printed onto a thin film of PI, and the PZT image together with connecting cables. The researchers reported that the harvester can generate a peak current ranging from 0.06 to 0.15 μA with a conversion efficiency of 1.7 %, which is sufficient to power the medical devices that motivated the work.

A single assembly essentially makes up a single PZT capacitor that charges when it is vibrated. The researchers organised the elements into 12 groups, a single group consisting of ten PZT capacitors connected in parallel and each group connected in series to increase the output voltage. Figure 10.16 displays the way the PZT capacitors

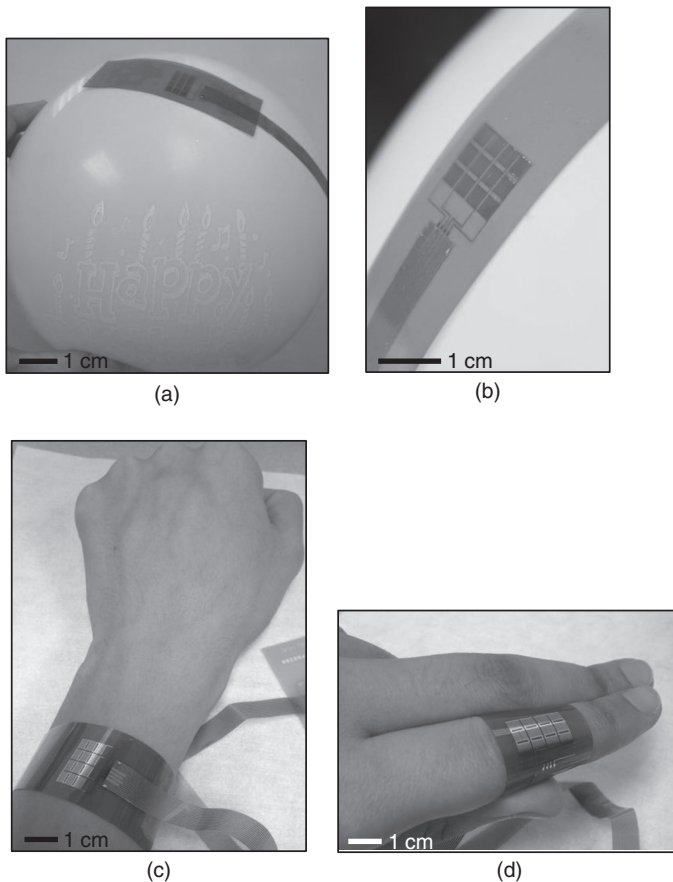


Figure 10.17 The flexibility of the PZT harvester and its conformity to various surfaces: (A) deployment on a balloon; (B) a magnified view of the harvester; (C) deployment on a human arm; (D) deployment of the harvester on a finger. Courtesy of Dagdeviren et al. (2014), *PNAS* (2014).

are organised, along with the electronic components that are required to condition the output voltage. Figure 10.17 displays the flexible deployment of the energy harvester on different objects.

References

- Beeby SP, Torah R, Tudor M, Glynn-Jones P, O'Donnell T, Saha C and Roy S 2007 A micro electromagnetic generator for vibration energy harvesting. *Journal of Micromechanics and Microengineering*, **17**(7), 1257.
- Beeby SP, Tudor MJ and White N 2006 Energy harvesting vibration sources for microsystems applications. *Measurement Science and Technology*, **17**(12), R175.
- Conway BE 2013 *Electrochemical Supercapacitors: Scientific Fundamentals and Technological Applications*. Springer Science & Business Media.
- Dagdeviren C, Yang BD, Su Y, Tran PL, Joe P, Anderson E, Xia J, Doraiswamy V, Dehdashti B, Feng X et al. 2014 Conformal piezoelectric energy harvesting and storage from

- motions of the heart, lung, and diaphragm. *Proceedings of the National Academy of Sciences*, **111**(5), 1927–1932.
- Dargie W 2012 Dynamic power management in wireless sensor networks: State-of-the-art. *Sensors Journal, IEEE*, **12**(5), 1518–1528.
- Erturk A and Inman DJ 2011 *Piezoelectric Energy Harvesting*. John Wiley & Sons.
- European Wind Energy Association 2016 Statistics webpage. URL: <http://www.ewea.org/library/statistics/offshore/>.
- Kansal A, Hsu J, Zahedi S and Srivastava MB 2007 Power management in energy harvesting sensor networks. *ACM Transactions on Embedded Computing Systems (TECS)*, **6**(4), 32.
- Khaligh A, Zeng P and Zheng C 2010 Kinetic energy harvesting using piezoelectric and electromagnetic technologies: state of the art. *Industrial Electronics, IEEE Transactions on*, **57**(3), 850–860.
- López-Lapeña O, Penella MT and Gasulla M 2010 A new MPPT method for low-power solar energy harvesting. *Industrial Electronics, IEEE Transactions on*, **57**(9), 3129–3138.
- Mitcheson PD, Yeatman EM, Rao GK, Holmes AS and Green TC 2008 Energy harvesting from human and machine motion for wireless electronic devices. *Proceedings of the IEEE*, **96**(9), 1457–1486.
- Nishimoto H, Kawahara Y and Asami T 2010 Prototype implementation of ambient RF energy harvesting wireless sensor networks. *Sensors, 2010 IEEE*, pp. 1282–1287–IEEE.
- Pandolfo A and Hollenkamp A 2006 Carbon properties and their role in supercapacitors. *Journal of Power Sources*, **157**(1), 11–27.
- Paradiso JA and Starner T 2005 Energy scavenging for mobile and wireless electronics. *Pervasive Computing, IEEE* **4**(1), 18–27.
- Qiu Y, Van Liempd C, Op het Veld B, Blanken PG and Van Hoof C 2011 5 μ w-to-10mw input power range inductive boost converter for indoor photovoltaic energy harvesting with integrated maximum power point tracking algorithm *Solid-State Circuits Conference Digest of Technical Papers (ISSCC), 2011 IEEE International*, pp. 118–120IEEE.
- Raghunathan V, Kansal A, Hsu J, Friedman J and Srivastava M 2005 Design considerations for solar energy harvesting wireless embedded systems *Proceedings of the 4th International Symposium on Information Processing in Sensor Networks*, p. 64.
- Ramadass YK and Chandrakasan AP 2010 A battery-less thermoelectric energy-harvesting interface circuit with 35 mV startup voltage. *IEEE Journal of Solid-State Circuits*. **46**(1), 333–341.
- Saha C, O'Donnell T, Wang N and McCloskey P 2008 Electromagnetic generator for harvesting energy from human motion. *Sensors and Actuators A: Physical*, **147**(1), 248–253.
- Shi Y, Xie L, Hou YT and Sherali HD 2011 On renewable sensor networks with wireless energy transfer *INFOCOM, 2011 Proceedings IEEE*, pp. 1350–1358.
- Sirohi J and Mahadik R 2011 Piezoelectric wind energy harvester for low-power sensors. *Journal of Intelligent Material Systems and Structures*, **22**(18), 2215–2228.
- Stanton SC, McGehee CC and Mann BP 2010 Nonlinear dynamics for broadband energy harvesting: investigation of a bistable piezoelectric inertial generator. *Physica D: Nonlinear Phenomena*, **239**(10), 640–653.
- Stephen N 2006 On energy harvesting from ambient vibration. *Journal of Sound and Vibration*, **293**(1), 409–425.

- Sudevalayam S and Kulkarni P 2011 Energy harvesting sensor nodes: Survey and implications. *Communications Surveys & Tutorials, IEEE*, **13**(3), 443–461.
- Tan YK and Panda SK 2011 Energy harvesting from hybrid indoor ambient light and thermal energy sources for enhanced performance of wireless sensor nodes. *Industrial Electronics, IEEE Transactions on*, **58**(9), 4424–4435.
- Taneja J, Jeong J and Culler D 2008 Design, modeling, and capacity planning for micro-solar power sensor networks *Proceedings of the 7th international Conference on Information Processing in Sensor Networks*, pp. 407–418.
- Vullers R, van Schaijk R, Doms I, Van Hoof C and Mertens R 2009 Micropower energy harvesting. *Solid-State Electronics*, **53**(7), 684–693.
- Winter M and Brodd RJ 2004 What are batteries, fuel cells, and supercapacitors? *Chemical Reviews*, **104**(10), 4245–4270.
- Zhu Y, Murali S, Stoller MD, Ganesh K, Cai W, Ferreira PJ, Pirkle A, Wallace RM, Cychosz KA, Thommes M *et al.* 2011 Carbon-based supercapacitors produced by activation of graphene. *Science*, **332**(6037), 1537–1541.